GPS Solut (2017) 21:1619–1631
DOI 10.1007/s10291-017-0638-1

ORIGINAL ARTICLE

Computation of GPS P1–P2 Differential Code Biases with JASON-2

Gilles Wautelet[1] · Sylvain Loyer[2] · Flavien Mercier[3] · Félix Perosanz[3]

Received: 13 December 2016 / Accepted: 5 May 2017 / Published online: 19 May 2017

Abstract GPS Differential Code Biases (DCBs) computation is usually based on ground networks of permanent stations. The drawback of the classical methods is the need for the ionospheric delay so that any error in this quantity will map into the solution. Nowadays, many low-orbiting satellites are equipped with GPS receivers which are initially used for precise orbitography. Considering spacecrafts at an altitude above the ionosphere, the ionized contribution comes from the plasmasphere, which is less variable in time and space. Based on GPS data collected onboard JASON-2 spacecraft, we present a methodology which computes in the same adjustment the satellite and receiver DCBs in addition to the plasmaspheric vertical total electron content (VTEC) above the satellite, the average satellite bias being set to zero. Results show that GPS satellite DCB solutions are very close to those of the IGS analysis centers using ground measurements. However, the receiver DCB and VTEC are closely correlated, and their value remains sensitive to the choice of the plasmaspheric parametrization.

Keywords GPS · Differential Code Biases · Plasmasphere · Total electron content

✉ Gilles Wautelet
Gilles.Wautelet@ulg.ac.be

[1] Institute of Astrophysics, Geophysics and Oceanography, University of Liège (ULg), Allée du Six Août 19C, 4000 Liège, Belgium

[2] Collecte Localisation Satellites (CLS), 11 Rue Hermès, 31520 Ramonville-Saint-Agne, France

[3] Centre National d'Etudes Spatiales (CNES), 18 Avenue Edouard Belin, 31401 Toulouse, France

Introduction

Hardware biases onboard GPS satellites and receivers are system parameters that need to be estimated while processing data for precise positioning applications. They physically correspond to a time delay due to the signal travel through the antenna and the different analog components like filters or amplifiers as well as to digital processing. Assessing the absolute values of hardware delays is very challenging; fortunately, most precise applications are based on signal combinations and need therefore to access the related combination delay. Among these is the so-called Geometry-Free combination which is mainly used to monitor the ionospheric total electron content (TEC). In precise positioning, measuring the ionospheric delay accurately is of crucial importance. For instance, the ionospheric models, like Global Ionospheric Maps (GIMs) which represent the TEC in two dimensions, are used to speed up the convergence time of real-time precise positioning (Banville et al. 2013) or to compute higher-order ionospheric effects (Hernández-Pajares et al. 2007). Scientific applications cover, for instance, the retrieval of the total plasmaspheric content in order to validate and improve ionospheric models like the International Reference Ionosphere, or IRI (Gulyaeva et al. 2002; Yizengaw et al. 2008).

TEC computation requires the knowledge of the dual-frequency combination of code delays, called Differential Code Biases (DCBs). Nowadays, the absolute TEC is known with an accuracy of several TEC units (TECU), where 1 TECU equals approx. 16 cm on GPS L1 frequency, and so are the derived GIMs (Hernández-Pajares et al. 2009). This limited accuracy is mainly due to the accuracy of satellite and receiver DCBs which, in turn, depends on the code precision. GPS DCBs refer to P-code

measurements recorded on the two legacy GPS frequencies L1 and L2, called P1 and P2, respectively. However, some receivers are not able to track the P-code either on one or both frequencies. To properly use the P1–P2 biases with such receivers (cross-correlated and C1, Y-codeless), there is the need to add a correction term which is accurately measured, distributed and known as the C1P1 DCB.

At the present time, there are two main ways of computing inter-frequency DCB values: They are estimated either simultaneously with the global or local ionospheric model or by assuming an a priori knowledge of the ionosphere to remove its contribution. In the first approach, DCBs are estimated together with the vertical TEC for a network of reference stations. The well-known example of such an approach is the production of Global Ionospheric Maps (GIMs). Part of the International GNSS Service (IGS), there are four Ionospheric Associate Analysis Centers (IAACs) which produce such maps and their related DCBs: CODE (Center for Orbit Determination in Europe, Astronomical Institute, consortium of Swiss and German research institutes and universities), ESOC (European Space Operations Center of ESA, Darmstadt, Germany), JPL (Jet Propulsion Laboratory, Pasadena, California, USA) and UPC (Technical University of Catalonia, Barcelona, Spain). For the sake of completeness, let us mention the specific DCB product computed by CODE: monthly values of satellite and receiver DCBs, whose daily repeatability is estimated at about 0.03 ns for the GPS P1–P2 bias. Another example is the methodology developed by the Chinese Academy of Science (CAS) which locally models the VTEC above each station of the network (Wang et al. 2015). Here the model is referred to as local since there is no global adjustment of the VTEC resulting from the DCB computation. The standard error for daily DCB solutions is the order of 0.1 ns in the case of GPS P1–P2 DCBs. The second approach subtracts the ionospheric delay in the line of sight of the satellite, called slant TEC, from code measurements. Montenbruck et al. (2014) use GIMs to extract the STEC for a network of reference stations in the context of multi-GNSS DCB computation. The corresponding products are daily solutions of satellite and receiver DCBs, characterized by a standard error of a few tenths of nanoseconds. In this method, the algorithm relies on the quality of the GIMs, which can strongly vary according to geomagnetic latitude and local time, notably.

Common to both approaches is the use of ground-based observations that are sensitive to the ionosphere and in particular to its fluctuations in time and space. Here we propose to compute DCBs from space-based measurements performed onboard the JASON-2 spacecraft, which is orbiting above the ionosphere at an altitude of 1350 km. In addition to satellite and receiver DCBs, VTEC above the satellite is also retrieved simultaneously in the same adjustment. This approach is innovative with respect to existing literature as previous studies focus either on VTEC or GPS satellite DCBs retrieval. On the one hand, to derive topside or plasmaspheric TEC, most studies consider GPS satellite DCBs as known values (Yue et al. 2011; Zakharenkova and Cherniak 2016), which implies that they derive ionospheric or plasmaspheric content using a product which is already affected by the ionosphere. On the other hand, if some studies have already developed a GPS satellite DCBs computation based on space-based measurements (Lin et al. 2016; Zhong et al. 2016), they generally eliminate the receiver DCBs from the adjustment process. The aim of this work is twofold: first, the validation of the existing ground-based products in a way that is insensitive to the ionospheric error by using space-based measurements. Second, it proposes an innovative solution to compute the VTEC and the receiver and satellite DCBs in a unique adjustment.

In the first section, the data and the DCB computation algorithm are presented. Then, the following section which presents the main results and the related discussion is divided into three parts. First, the analysis of a single case is presented, and then, the sensitivity of DCB solution to the algorithm parametrization is studied. At last, the stability of a 30-day DCB computation is assessed and discussed. Finally, we conclude and propose some improvements and perspectives.

Data and methodology

DCBs are computed in two different ways. The first, which will be further referred to as "ground solution," is based on a network of permanent stations belonging to the Multi-GNSS Experiment of the IGS (MGEX). The method is similar to that developed in Montenbruck et al. (2014), which uses GIMs to compute the slant TEC for a given line-of-sight. In comparison with the original implementation of Montenbruck et al. (2014), we have slightly modified two parameters: the elevation cutoff angle has been increased from 20° to 30° and the computation of the mixed DCBs (satellite and receiver) is achieved through a weighted mean (instead of an arithmetic one), the weights being proportional to satellite elevation. The network used consists of about 40 stations equipped with semi-codeless receivers only, meaning that no C1P1 bias has to be applied. The GIM used is the combined IGS solution with the appropriate mapping function, which is the classical thin single-layer model (Klobuchar 1996). Comparison of our implementation with the original results published by DLR (available at ftp://cddis.gsfc.nasa.gov/gnss/products/mgex/dcb/) shows very little differences, which are in the order of magnitude of the DCB precision. These ground-

based data have been obtained for validation purpose only, as the goal of this work is the computing DCBs based on space-based measurements.

The second DCB dataset is called "space solution" and is related to GPS data recorded by the Global Positioning System Payload (GPSP) instrument onboard the JASON-2 satellite. GPS code and phase measurements are available in RINEX format from the AVISO ftp server (ftp://avisoftp.cnes.fr/AVISO/pub/doris/jason-2) dedicated to satellite altimetry data. The methodology used to compute DCBs from JASON-2 measurements is described below.

Since DCBs are related to code measurements only, no processing of the phase has been used in the following algorithm. Let us note that JASON-2 directly provides P-code measurements so that there is no need to use the C1P1 bias mentioned earlier.

First, the Geometry-Free (GF) combination of pseudo-range observations P_1 and P_2, called P_{GF}, is formed for each satellite pass and is expressed in meters:

$$P_{GF} = P_1 - P_2 = \alpha \mathrm{STEC} + M_{GF} + \mathrm{DCB}^i + \mathrm{DCB}_r + \varepsilon_{GF} \quad (1)$$

with α being numerical coefficient relating to GPS L1 and L2 frequencies, $\alpha = -1.05{,}046\ 10^{-17}$ (m^3/e^-), STEC is the slant total electron content in units of TECU, M_{GF} is the multipath error term in the GF combination, DCB^i and DCB_r are the DCBs related to the GPS satellite and the JASON-2 receiver, respectively, and ε_{GF} is the noise of the GF combination. In Eq. (1), DCBs are expressed in meters but we will further express them in nanoseconds to be consistent with the existing literature and the IGS community.

As STEC corresponds to the integral of the electronic density along the receiver-to-satellite path, it corresponds in this case to the plasmaspheric content between the altitude of JASON-2 (1350 km) and that of GPS satellites (20,200 km). The relation between the slant and the vertical TEC is given by the geometric mapping function (Xu 2003):

$$\mathrm{STEC} = \mathrm{MF}\,\mathrm{VTEC}$$
$$\mathrm{MF} = -\left(\frac{R_e + h}{H}\right)\cos(z) + \frac{\sqrt{(R_e + h + H)^2 - (R_e + h)^2 \sin^2(z)}}{H} \quad (2)$$

with R_e the earth's radius, h the altitude of the spacecraft, H the upper altitude of the plasmasphere and z the zenith angle of the GPS satellite observed from the spacecraft.

The geometric mapping function can be used if a height-dependent homogeneous distribution of free electrons is assumed, which is the case in the plasmasphere where the exponential decrease is assumed. In our case, we consider the plasmasphere as a thick layer extending from the spacecraft to an upper altitude H. To reduce the mapping function error, an elevation cutoff of 30° has been applied. The choice of this value is justified in the next section.

Considering n GPS satellites observed simultaneously by the onboard receiver, the linear model for a given observation epoch is written as follows:

$$\begin{pmatrix} P^1_{GF} \\ P^2_{GF} \\ \vdots \\ P^n_{GF} \end{pmatrix}_{n\times 1} = \begin{pmatrix} \alpha\mathrm{MF}^1 & 1 & 0 & \dots & 0 & 1 \\ \alpha\mathrm{MF}^2 & 0 & 1 & \dots & 0 & 1 \\ \vdots & \vdots & \vdots & \vdots & \vdots & \vdots \\ \alpha\mathrm{MF}^n & 0 & 0 & \dots & 1 & 1 \end{pmatrix}_{n\times(n+2)} \begin{pmatrix} \mathrm{VTEC} \\ \mathrm{DCB}^1 \\ \mathrm{DCB}^2 \\ \vdots \\ \mathrm{DCB}^n \\ \mathrm{DCB}_r \end{pmatrix}_{(n+2)\times 1} \quad (3)$$

with MF^i being the mapping function related to the GPS satellite i.

Equation (3) has more unknowns than observation equations, which means that the system is under-determined. Considering that both the satellite and receiver DCBs are stable within 1 day, stacking of equations over several observation epochs will overdetermine the problem and allow estimation through a least-squares adjustment. However, the system needs an additional constraint called "zero-mean average" which will serve as reference for the biases (Montenbruck et al. 2014). Here we constrain the sum of satellite DCBs for the whole GPS constellation (32 satellites) to be equal to zero.

The associated stochastic model is a classical weighting of the observations as a function of the GPS satellite elevation. The weight of a given observation W_i is proportional to the sine of the GPS satellite elevation: $W_i = \frac{1}{\sigma^2}\sin(e_i)$, with σ^2 being the a priori variance of a code observation (the precision is assumed to be equal to a hundredth of P-code wavelength) and e_i the elevation of the satellite i.

Finally, for a given day, the number of estimated parameters from the global adjustment equals the number of VTEC values, corresponding to the number of observation epochs plus the 33 values of DCBs (32 satellites plus the receiver) which are computed as daily constants.

Results and discussion

In a first step, we will present the results related to 2 days of data: Days Of Year (DOY) 263 and 240 in 2015, which are close to the autumn equinox. As the solution may depend on the parametrization of the ionospheric model, i.e., the cutoff angle and the mapping function, a sensitivity study will be presented in a second step. At last, a monthly solution will be built, and its stability will be discussed.

Example of a daily solution

Since 2010, the CNES-CLS Analysis Center (AC) in Toulouse (France) provides orbit and clock solutions for precise positioning applications, such as integer-fixed Precise Point Positioning (Loyer et al. 2012), and the related products, called GRG, that participate to the IGS final products. To follow the naming convention, we will further refer to our ground-based solution as GRG-ground and to our space-based solution (JASON-2) as GRG-LEO.

Figure 1 shows the DCB^i difference between the daily C1W–C2W (or P1–P2) GRG-LEO solution for DOY 263, 2015, and the solutions provided by the IGS analysis centers CODE (Center for Orbit Determination in Europe, Germany and Switzerland), CAS (Chinese Academy of Science, China) and DLR (Deutsches Zentrum für Luft- und Raumfahrt, Germany) in addition to our GRG-ground solution (GRGg). The parameter values chosen are 30° elevation cutoff angle and a plasmaspheric height of 2000 km (see Eq. 2). The first value comes from the fact that the GPSP antenna is tilted by 15° with respect to the spacecraft axes (AVISO website). It causes the antenna zenith not to correspond to the local vertical, which is the reference for computing elevation and VTEC. Therefore, a value of 30° elevation cutoff ensures, in the opposite directions of the along-track component, to track GPS satellites at minimum 15° and 45° in the antenna reference frame. The value of 15° can be considered as a reasonable threshold with respect to multipath error and measurement noise. The plasmaspheric height of 2000 km has been chosen as a realistic value given the exponential decrease in the H+ concentration in the plasmasphere: It is generally admitted that H+ scale height in the low plasmasphere lies between 500 and 3000 km (Marinov et al. 2015). Since the plasmaspheric height related to the geometric mapping function is defined as "the first two scale heights above the surface" (Foelsche and Kirchengast 2002), we fixed it at 2000 km. As already mentioned, the influence of elevation and plasmaspheric height on DCB retrieval will be investigated in a second part.

For the GRG-LEO solution, the mean standard error related to the GPS DCB^i is 0.023 ns while the standard error for JASON-2 receiver DCB is 0.067 ns. The largest standard error is found for PRN10 (G10), reflecting the lowest number of observations related to that spacecraft; it has been observed for one observation period of about 20 min only, in comparison with 11 observation periods for the other PRNs. Let us mention that the standard error related to ground-based solutions is generally in the range 0.05–0.06 ns for DCB^i. Therefore, the GRG-LEO values are found to be particularly low with respect to other ground-based solutions for which many GNSS permanent stations are used within the computation.

An analysis of Fig. 1 shows that discrepancies between solutions are generally larger than the standard error of the GRG-LEO estimate. However, let us point out that such differences are normal distributed: For instance, the difference (GRG-LEO − GRGg) has a null average and a standard deviation of 0.349 ns. The quasi-null average means that our space-based solution is unbiased with respect to the other solutions. Table 1 shows the root mean square (RMS) of the difference between the solutions. Its analysis reveals that GRG-LEO solution is consistent with other AC solutions and with the GRG-ground solution. Indeed, the differences of the GRG-LEO solutions have the same order of magnitude as do discrepancies between ACs. The results in Table 1 show that differences including CAS are the largest, meaning that this AC proposes the most

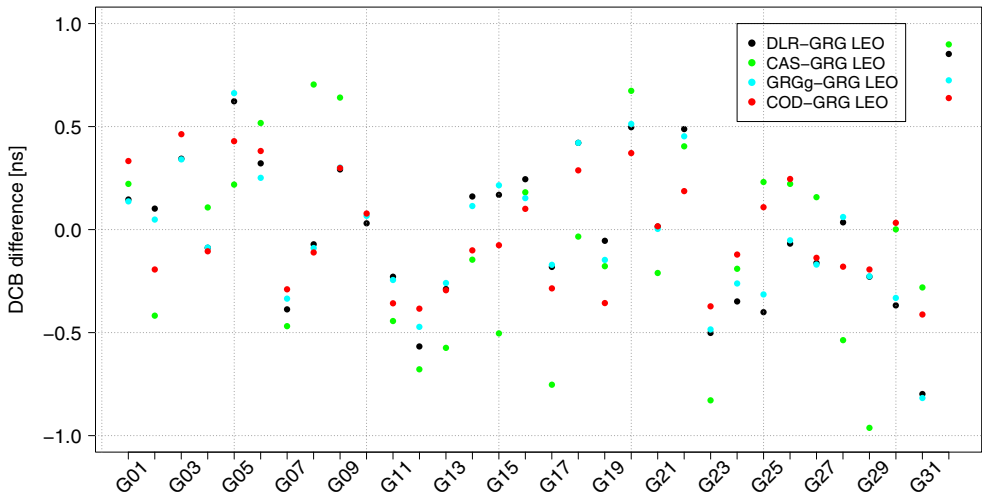

Fig. 1 DCB^i difference between GRG-LEO C1W–C2W (or P1–P2) solution for DOY 263, 2015, and our ground-based solution (GRGg) or other IGS analysis centers DLR, CODE and CAS

Table 1 Root mean square (RMS) of the difference between DCB^i solutions for DOY 263, 2015, expressed in nanoseconds

	GRG-ground	COD	DLR	CAS
GRG-LEO	0.344	0.287	0.366	0.521
GRG-ground	–	0.192	0.050	0.410
COD	–	–	0.213	0.333
DLR	–	–	–	0.408

different DCB^i solutions. On the contrary, our ground solution GRGg and DLR agree very well, due to the use of the same methodology.

DCBs are not the only product of our global adjustment. The VTEC at each observation epoch is also computed. It is interesting to investigate its behavior and assess how realistic are the estimated values. Figure 2 depicts the evolution of the VTEC during a complete revolution of JASON-2 (about 1 h 52 min) for DOY 240, 2015 (August 28). Let us recall that these values are expected to have a decimeter-level accuracy due to the nature of code measurements. DOY 240, 2015, is characterized by an active geomagnetic and solar activity, with K_p values ranging from 3 to 6 and a daily solar flux at 10.7 cm (F10.7) of 109 s.f.u. (solar flux units).

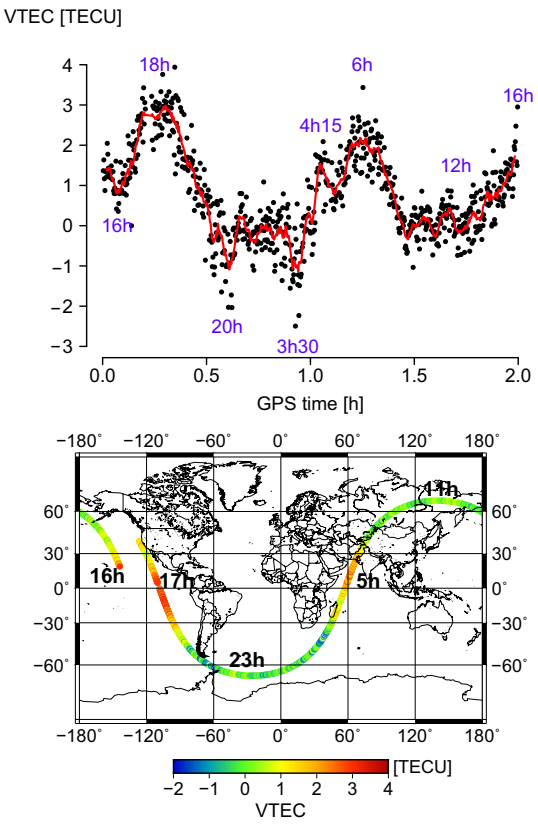

Fig. 2 *Top* Time series of VTEC, expressed in TEC units (TECU), for the first revolution of JASON-2 on DOY 240, 2015. *Black dots* depict unsmoothed VTEC values (i.e., the raw by-product of the least-squares adjustment) while the *red line* corresponds to 1-min running average. Local time for the spacecraft is shown in *blue*. *Bottom* Map of VTEC values corresponding to the first revolution of JASON-2. Local time (LT) is mentioned for the points of interest (high latitudes and equator crossings)

The VTEC noise assessed based on Fig. 2 is in the order of 1–2 TECU, which means between 15 and 30 cm on L1 frequency. This order of magnitude is in good agreement with theoretical noise value, generally assumed to correspond to one-hundredth of the P-code wavelength. The measurement noise can be mitigated by applying a 1-min running average, which allows highlighting the following patterns due to the plasmasphere morphology: (1) At the beginning of the arc, early evening crossing of the magnetic equator (1700–1800 LT) can be easily identified with the largest VTEC values of the period. (2) Then, the satellite flew over mid- and high latitudes in the southern hemisphere during nighttime, with very small VTEC and minimum above the Antarctic Circle. (3) In the morning hours, one can observe a double peak in VTEC (0415 and 0600 LT), which could be the signature of the equatorial anomaly in the plasmasphere. (4) At last, even during daytime, the crossing of high latitude regions (around 1100 LT) shows very little contribution of the plasmasphere, with values being nearly the order of nighttime ones for the same region.

The amplitude of VTEC values is about 6 or 4 TECU, considering raw (black dots) or smoothed (red line) values, respectively. This is consistent with previous plasmaspheric content studies, like in Lee et al. (2013) where authors observed plasmaspheric TEC between 2 TECU at high latitudes and 8–10 above equatorial regions during similar solar and geomagnetic conditions ($F10.7 > 100$ and $K_p > 2.5$). Nevertheless, even though the VTEC ranges agree well with the literature, some of the VTEC values appearing in Fig. 2 are negative, which has no physical meaning. Therefore, DCBs of either GPS satellites or JASON-2 receiver are underestimated in our algorithm.

Sensitivity analysis

Parametrization is important to give physical meaning to the model while keeping low model residuals and a good observability of the phenomenon. This section investigates the impact of the elevation cutoff angle on DCB retrieval first, followed by the study of the influence of the plasmaspheric model.

Elevation cutoff angle

Figure 3 shows the DCB solution for JASON-2 receiver and GPS satellite PRN32 as a function of elevation cutoff angle for DOY 240, 2015. Let us note that similar results have been obtained for all GPS satellites so that the case of

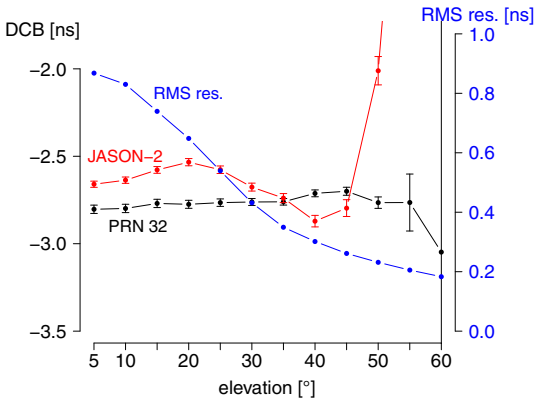

Fig. 3 DCBs obtained with the GRG-LEO algorithm for several elevation cutoff angles on DOY 240, 2015. The plasmaspheric height is set to 2000 km. The *black dots* and the associated *error bars* (representing the standard error) are related to GPS satellite PRN32 while the *red dots* concern the JASON-2 receiver DCB. In addition, mean RMS of residuals is depicted in *blue* (scale on the *right axis*)

PRN32 is used here for illustrating purpose, without any loss of generality. One can observe that PRN32 DCB^i shows little variation with elevation cutoff angle from 5 to about 35°, the value from which the elevation exerts a non-negligible influence. Moreover, if we consider angles lower than 50° or 55°, we can see that the standard error on DCB^i estimation is similar for all elevation values. For angles larger or equal to 55°, the stability of the solution is not guaranteed anymore, showing a significant decrease in the DCB^i and a clearly larger associated error bar. Therefore, considering elevation values smaller than 50 degrees, one can conclude that the cutoff angle has little impact on DCB^i estimation and precision.

Turning to receiver DCB_r (JASON-2 GPSP receiver), the conclusions are quite different: There is a clear dependence of the DCB_r on the cutoff angle, and the amplitude of variations is larger than the standard error on the DCB_r itself. The DCB_r variation is the order of 0.2–0.3 ns for elevations smaller than 50° but rises rapidly beyond, with values reaching about 2.7 ns, while a solution related to a 20° elevation threshold gives a DCB_r value of −2.8 ns. These extremely variable DCB_r are compensated by a shift of the estimated VTEC values. Indeed, the larger the elevation cutoff angle, the more VTEC and DCB_r are correlated. In this manner, it becomes very difficult to distinguish these two contributions in a single adjustment. Therefore, the ideal elevation value should be low enough to allow the decorrelation of VTEC and DCB_r.

Figure 3 also depicts the mean root mean square (RMS) of residuals for each elevation value, which exhibits a decrease with elevation cutoff angle. The slope is nearly constant from 5° to 35°, where each 5° slice leads to an RMS gain of 0.1 ns. From 35° and beyond, the gain is less important with a slope being about three times smaller.

The best choice of the elevation cutoff angle should, therefore, be a compromise between the precision of the estimates, low residual RMS values, and realistic DCB values for both satellites and receiver. Given these constraints, we chose to fix the elevation cutoff value at 30° in our algorithm. In addition, let us recall that, due to the 15° antenna tilt, a cutoff value smaller than 15° would imply elevations below 0° (boresight angles >90°) in the antenna reference frame, with increased noise and multipath error. The preferred values should, therefore, be larger than 15° or 20° to ensure mitigated tracking error and noise.

Plasmaspheric model

To convert slant TEC values to the vertical, we formerly took a geometric mapping function with a plasmaspheric height of 2000 km. In this section, we will investigate the effect of varying this height or considering another mapping function.

Figure 4 (*top left*) shows DCBs for JASON-2 receiver and PRN32 for several plasmaspheric heights H for DOY 240, 2015, with the elevation set to 30°. Like previously, PRN32 illustrates the general behavior of all DCB^i. We can see that the PRN32 DCB does not change with plasmaspheric height, which is not the case of the JASON-2 DCB which exhibits a linear relationship with this parameter. In addition, the standard error on the JASON-2 DCB is also increasing with plasmaspheric height while this does not seem to be the case for PRN32 DCB. The daily mean of RMS residuals is also plotted in Fig. 4 (*top left*), where one can see that the value of H does not influence the quality of the fit. Therefore, considering a same level of residuals, the change in DCB_r must be compensated by another parameter, which is presently the VTEC.

Figure 4 (*top right*) shows the time series of VTEC for the first 2 h of DOY 240, 2015 (approximately the first revolution of JASON-2 for that day), and for several values of the plasmaspheric height. One can immediately notice the shift related to the change of DCB_r: The difference of −0.5 ns between 1000 and 15,000 km is compensated by a VTEC shift of about +1 TECU. Knowing that 1 TECU equals about 16 cm and that 1 ns equals 15 cm, we can see that all the solutions are equivalent in terms of residuals, which is translated into the constant RMS value visible in Fig. 4 (*top left*). As already mentioned, negative VTEC values are physically impossible so that the selected value of the plasmaspheric height should be the one that leads to null values during periods of VTEC minimum, i.e., at 0.6 and 0.9 GPS time in Fig. 4 (*top right*). These periods correspond to the crossing of mid-/high-latitude plasmasphere during nighttime (around 2000 LT and 0330 LT, respectively, see Fig. 2). In this case, the preferred H value would correspond to 15,000 km.

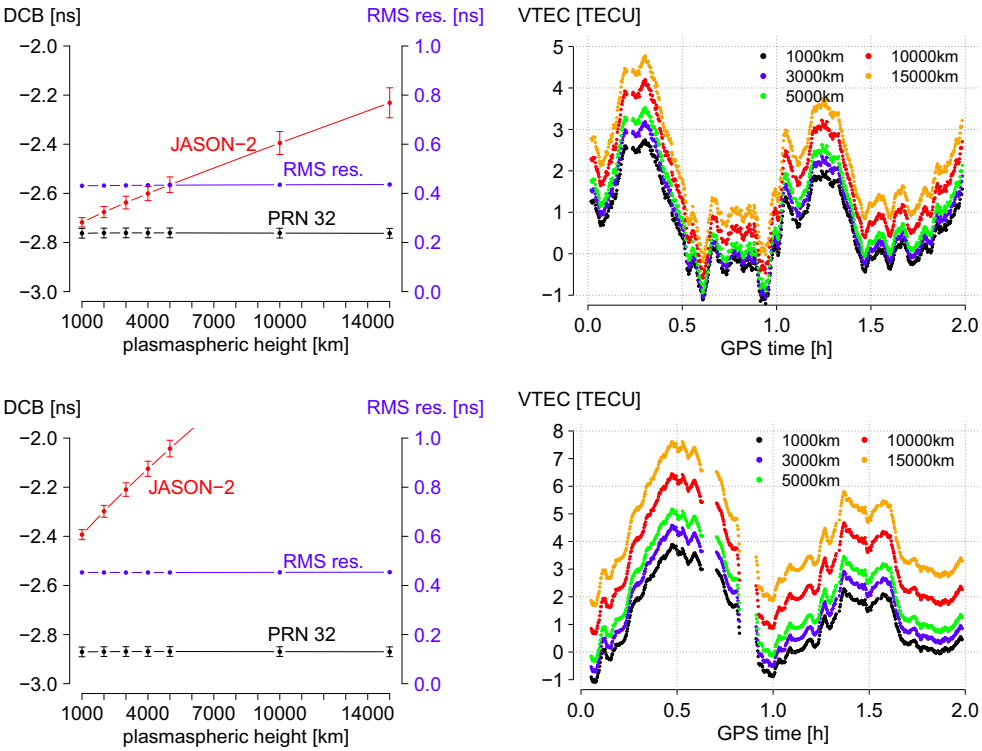

Fig. 4 Sensitivity test of the geometric mapping function considering several plasmaspheric heights for DOYs 240 (*top*) and 246 (*bottom*). The elevation cutoff angle is set to 30°. *Left* DCBs for GPS PRN32 and JASON-2 receiver as a function of plasmaspheric height and mean of RMS residuals (related to *right axis*). *Right* Time series of 1 min averaged VTEC for the first 2 h considering several plasmaspheric heights

Figure 4 (*bottom*) presents the same analysis 1 week later, on DOY 246, 2015. The linear relationship between DCB_r and the plasmaspheric height is very different from that related to DOY 240, 2015: The solution is clearly more sensitive to the value of the plasmaspheric height. Indeed, the DCB_r value corresponding to $H = 15{,}000$ km (which is outside of the plotting area) is about -1.3 ns, which represents a difference of more than 1 ns with respect to $H = 1000$ km. Considering the minimum VTEC $= 0$ condition, we can see from Fig. 4 (*bottom right*) that $H = 5000$ km is here the appropriate value. Because of the orbit plane precession, the local time corresponding to the first orbit is shifted by approximately 90 min with respect to DOY 240, 2015, so that the VTEC time series present markedly different patterns. For instance, the first maximum observed at 0030 GPST corresponds to approximately 1500 LT, instead of 1800 LT for DOY 240, 2015. The dynamics of the VTEC observed can, therefore, be enhanced or reduced due to the phase of the orbit plane, which affects the appropriate value of H considering a null value at the VTEC minimum. As a consequence, finding out an appropriate value for H that suits all orbit phases looks very challenging, especially if polar regions, where the minimum is expected to be observed, are crossed during the daytime. Indeed, it seems that the H parameter actually varies, so that future developments of the algorithm may concern a model of this parameter to take into account its latitude and local time dependence, notably. Nevertheless, like for DOY 240, 2015, let us highlight that the GPS satellite DCB solution is still insensitive to this parameter.

The same analysis can be conducted using another simple mapping function found in the literature since the beginning of ionospheric studies with GNSS: the single-layer model, or SLM (Klobuchar 1996; Hofmann-Wellenhof et al. 2001). Generally used for the ionosphere, the model approximates a 3-D layer into a single shell located at a representative altitude where all ions are supposed to be contained in. For instance, the ionospheric thin layer is generally located at an altitude between 350 and 450 km, which corresponds to several times the scale height of the ionosphere, depending on season, local time and solar activity (Liu et al. 2006). Adapted to the JASON-2 altitude, the model will consider a plasmaspheric single layer at an altitude above 1350 km. Given the exponential decrease in the plasmaspheric content, which differs from the vertical profile of the ionosphere exhibiting a density peak, there is the need to test the sensitivity of the algorithm to this parameter by considering a shell height above the receiver ranging from 1000 to 15,000 km.

Figure 5 presents similar results as in Fig. 4, except that the mapping function related to the SLM is computed as follows, using the same naming convention than in (2):

$$\mathrm{MF} = \frac{1}{\sqrt{1 - \left(\frac{R_e}{R_e + h}\sin(z)\right)^2}} \tag{4}$$

with h the plasmaspheric shell height, expressed in kilometers.

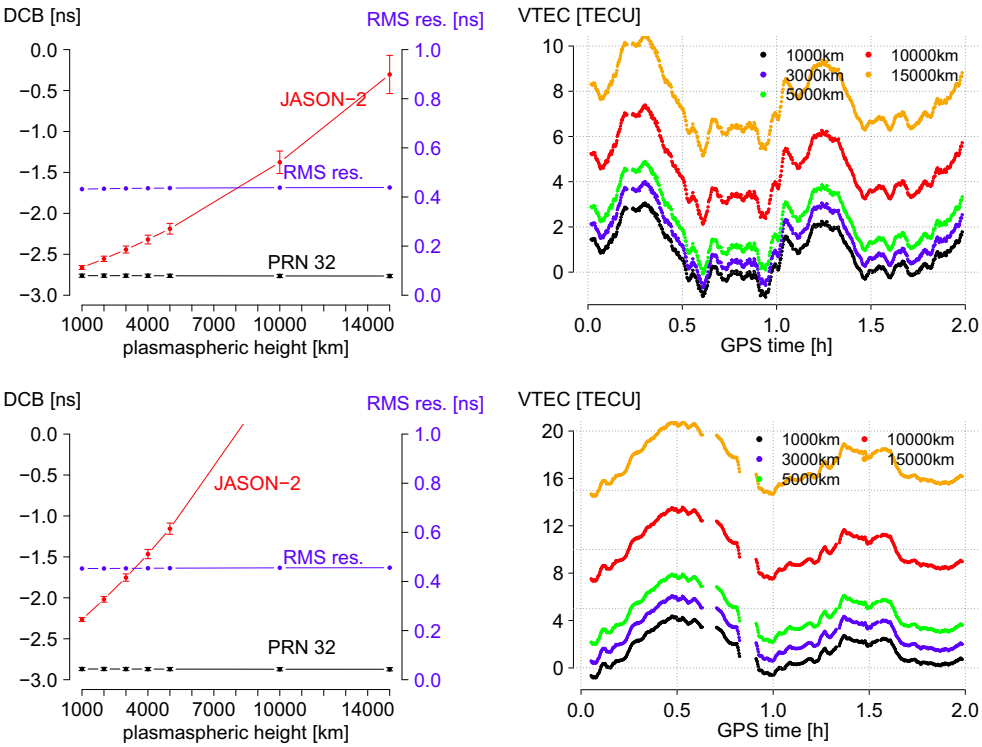

Fig. 5 Sensitivity test of the single-layer model (SLM) considering several plasmaspheric shell heights for DOYs 240, 2015 (*top*), and 246, 2015 (*bottom*). The elevation cutoff angle is set to 30°. *Left* DCBs for GPS PRN32 and JASON-2 receiver as a function of the shell height and mean of RMS residuals (related to *right axis*). *Right* Time series of 1 min averaged VTEC for the first 2 h considering several shell heights

An analysis of Fig. 5 shows very similar results to Fig. 4, for instance, the linear increase in the receiver DCB with the plasmaspheric shell height and the steepest slope for DOY 246, 2015, compared with 240, 2015. However, considering a given day, the difference between DCB related to extreme values 1000 or 15,000 km is markedly larger than using the geometric model (more than 2 ns and about 0.5 ns, for SLM and geometric mapping function, respectively, on DOY 240, 2015), even if one recognizes that a plasmaspheric height of 15,000 km is completely unrealistic. Comparison of Figs. 4 and 5 shows that some parametrizations give equivalent solutions, like the geometric mapping function with $H = 15{,}000$ km and the SLM model with $h = 5000$ km for DOY 240, 2015. However, given that both solutions are equivalent in terms of error bar and the larger sensitivity of the SLM, it is proposed to use the geometric mapping function, keeping in mind that the choice or the development of a model of the H parameter is an important issue while assessing VTEC and DCB_r.

As a conclusion, the proposed algorithm will consider the methodology described in the previous section with an elevation cutoff of 30° and the geometric mapping function with a plasmaspheric height at 15,000 km, knowing that the latter value should be adapted and will change both the DCB_r and VTEC estimates.

Solution stability

Taking into account the methodology and parametrization previously mentioned, the algorithm has been applied on 30 days of JASON-2 RINEX files to compute daily DCBs for both GPS satellites and receiver: The period analyzed is DOY 240–269 (28 August to 26 September) in 2015. The time series of GPS satellite DCBs is shown in Fig. 6 while the receiver solution is depicted in Fig. 8, considering a DCB alignment based on a 32 GPS satellites solution. The alignment procedure consists in applying a shift to a non-32 satellite DCB solution to align it to the reference day. This shift corresponds to a mean bias computed using all common satellites, which is added to all DCB^i and subtracted to the DCB_r.

GPS satellites DCBs

In order to infer any DCB drift with time, regression lines for each satellite have been computed. For all satellites, the slope of the regression is not statistically different from zero, meaning that GPS DCBs can be considered stable within the time period. Assuming the fact that daily solutions are independent, i.e., there is neither a priori information nor constraint on the estimates, the stability in time is expressed in terms of standard deviation. Stability values vary between about 0.04 ns (e.g., PRN04) and 0.18 ns (e.g., PRN 05), with a

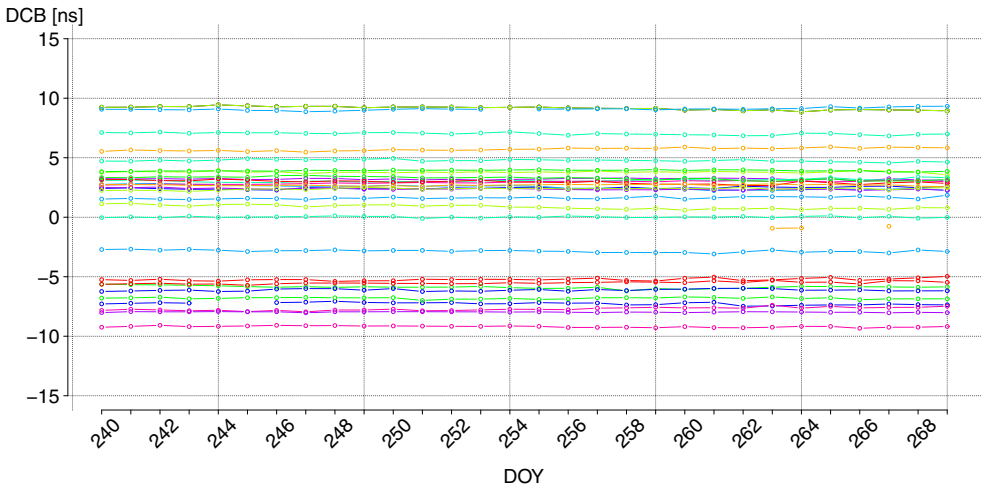

Fig. 6 GPS satellite DCBs for DOY 240–269 in 2015, using an elevation mask of 30° and a plasmaspheric height (geometric MF) of 15,000 km. All daily solutions are aligned on DOY 263 for which all 32 satellites of the GPS constellation were observed

mean value of approximately 0.1 ns. These values are compared with those computed by DLR and CAS analysis centers and also with our GRG-ground solution (Fig. 7).

Figure 7 shows a larger dispersion for the GRG-LEO than for other solutions, and in particular with respect to DLR which exhibits the best stability (smallest values). Despite this, our space-based solution using a single receiver offers stability comparable to that of methods relying on a ground network of several tens of stations. Therefore, one can expect that using several LEO satellites like JASON-2 can improve the solution stability to make it comparable to ground-based solutions.

JASON-2 receiver (DCB_r)

Figure 8 displays the daily DCBs related to JASON-2 receiver for the same period, i.e., DOY 240–269 in 2015.

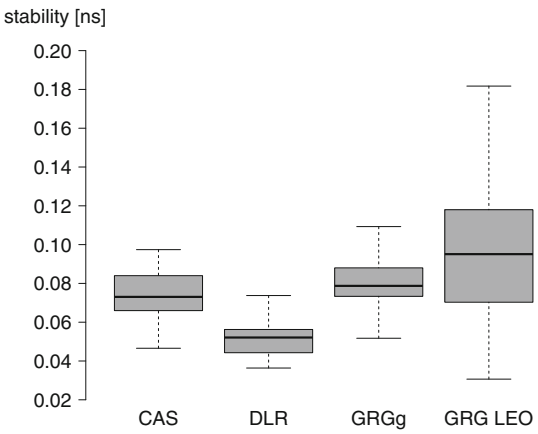

Fig. 7 *Boxplot* of the GPS satellite stability based on 30 days for GRG-LEO and GRG-ground, DLR and CAS analysis centers. *Box* bounds correspond to quartiles (P_{25} and P_{75}) while the thick line is the median. *Whiskers* are located at $P_{25} - 1.5$ IQR (interquartile range) and at $P_{25} + 1.5$ IQR. If this value exceeds the minimum (maximum) of the dataset, the *whisker* is located at the minimum (maximum)

The magnitude of the variations is of order 1 ns, which is clearly larger than the DCB_r standard error. We can clearly see an increase of nearly 1 ns in about 7 days, before coming back to the initial value of DOY 240, followed by shorter-term variations until the end of the studied period. Let us mention that such variations are not, as is the case for GPS DCBs, due to the variable number of GPS satellites in the constellation because all solutions have been aligned on the 32-satellites period, which corresponds to DOYs 263, 264 and 267.

Since it has already been suggested that space-based receiver DCBs may depend on the receiver temperature (Yue et al. 2011), we have plotted the temperature values obtained from different temperature probes of the GPSP-B receiver onboard JASON-2 in Fig. 9. Even if all absolute values differ, they all show the same variation with time: for instance, the rather sharp increase around DOY 259, whose signature is similar to that of an eclipse period. Let us note that the noise of the time series corresponds to small temperature changes at the orbit period so that the latter is not the cause of the variations observed in Fig. 9. Comparison of receiver DCB and temperature variations shows that there is very little correlation between these variables, suggesting that other phenomena are responsible for the observed variations in JASON-2 receiver.

As already mentioned, receiver DCB and VTEC are closely correlated, so that changes in the plasmaspheric properties are mapped into both estimates. Since we considered a constant parametrization of the plasmaspheric model ($H = 150{,}000$ km), plasmaspheric changes during the 30-day period could explain the high variability in receiver DCB solution. Such changes are generally due to variations of geomagnetic and solar conditions, which are plotted in Fig. 10 for the period of interest. While the planetary K value (K_p) and Disturbance Storm Time (DST) indices are representative of geomagnetic conditions observed from high and low latitudes, respectively, the

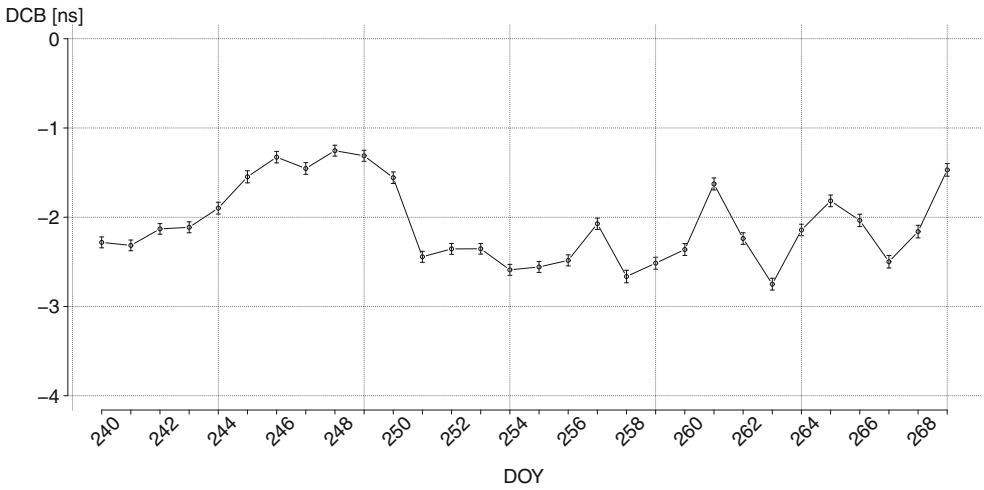

Fig. 8 JASON-2 receiver DCB for DOY 240–269 in 2015, using an elevation mask of 30° and a plasmaspheric height (geometric MF) of 15,000 km. All daily solutions are aligned on DOY 263 for which all 32 satellites of the GPS constellation were observed

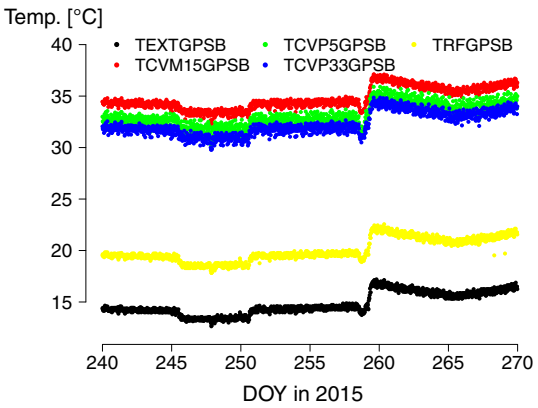

Fig. 9 Time series of temperature obtained from the different temperature probes of the GPSP-B instrument onboard JASON-2, for DOYs 240–269 in 2015. (*credits*: G. Zaouche, CNES)

solar radio flux at 10.7 cm (F10.7) is a proxy of solar activity, greatly correlated with the extreme ultraviolet (EUV) irradiance responsible for ionization of the plasmasphere.

Even though the comparison of Figs. 8 and 10 can reveal some clues of anticorrelation between DCB_r and geomagnetic activity during the first 10 days (DOY 240–250), a quick look at the whole period shows that there is little relationship between these variables, like for temperature measurement. Correlation of daily values between DCB_r and DST, K_p and F10.7 is 0.43, −0.28 and −0.28, respectively, which is statistically not significant. If the plasmaspheric response to geomagnetic storms or substorms can be understood as a smooth recovery, what is the response during the occurrence of repeated events, like between DOYs 251 and 255, where several strong DST depletions were observed? In addition to the geomagnetic context, let us recall that ionization in the plasmasphere is partially driven by EUV fluxes coming from solar activity and translated through the F10.7 radio flux.

Therefore, the interactions between geomagnetic conditions, solar background, and plasmaspheric content seem too complex to be simply described by a single parameter, such as the plasmaspheric height H so that the plasmaspheric model described in this work is not sufficient to be used for concurrent receiver DCB and plasmaspheric studies. Nevertheless, let us note that GPS satellite DCBs were almost insensitive to plasmaspheric model and parameterization, meaning that our methodology is still valid for satellite DCB computation based on space measurements only.

Conclusion and perspectives

We describe a DCB computation method based on space-based GPS observations onboard the JASON-2 spacecraft which is located above the ionosphere. The proposed algorithm allows to compute not only satellite and receiver DCBs at the same time but also to assess the plasmaspheric VTEC above the satellite, thanks to a simple plasmaspheric model assuming a constant thickness. Comparison of our satellite solutions with that of Analysis Centers (ACs) of the IGS shows that the formal error on the estimates is of the same order of magnitude (about 0.05 ns) while the difference of our solution with other AC solutions shows discrepancies of 0.3 ns on average, which is similar to discrepancies between ACs themselves. These results seem to prove that the ionosphere has a minor impact on ground-based products proposed by the IGS.

A sensitivity study has demonstrated that if both elevation cutoff angle and plasmaspheric model influence onboard receiver DCB and VTEC, only the cutoff value impacts the GPS satellite DCB solution. In conclusion, the method proposes an alternative to algorithms based on ground station measurements, which rely on the a priori knowledge of the ionospheric content at any location, with

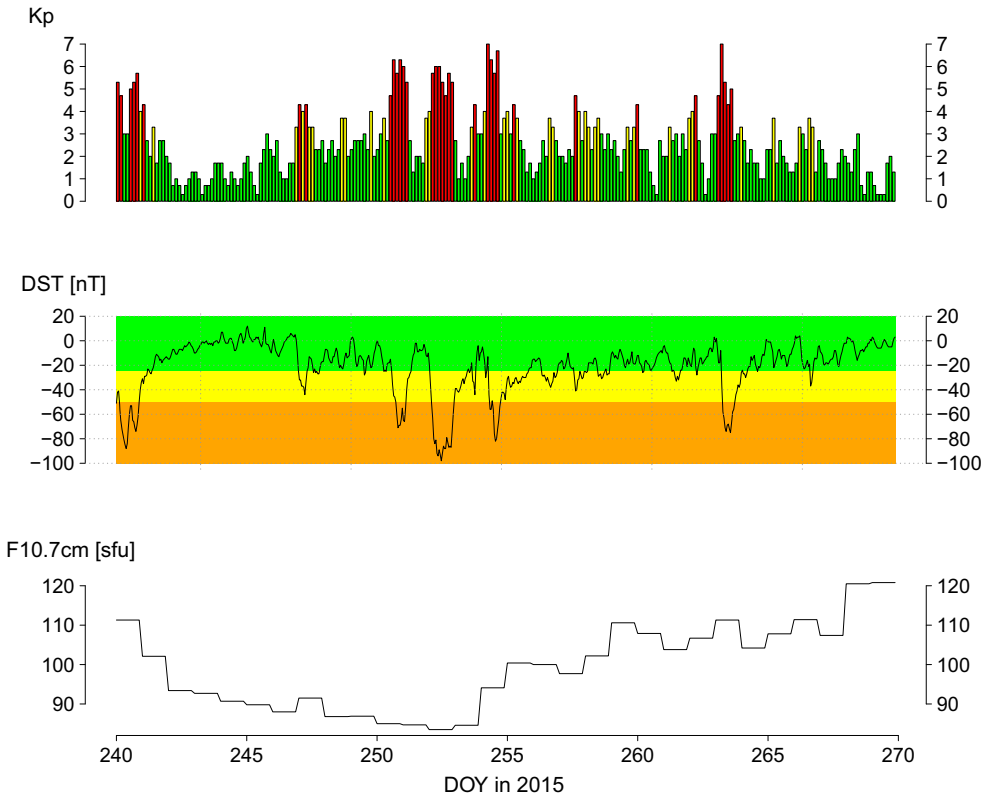

Fig. 10 Geomagnetic and solar indices from DOY 240–269 in 2015. *Top* Planetary K value (K_p) *Middle* Disturbance Storm Time index (DST) *Bottom* Solar radio flux at 10.7 cm. (*Sources*: https://www.ngdc.noaa.gov for K_p and F10.7 and http://wdc.kugi.kyoto-u.ac.jp for DST)

a DCB precision similar to that of IGS ACs. The main drawback of this all-in-one DCBs/VTEC computation is that the plasmaspheric model is not complex enough to discriminate and estimate correctly receiver DCB and VTEC, which are closely correlated.

Improvements of our method concern the simultaneous use of several LEO satellites orbiting either at the same altitude, like JASON-2 and 3, or at lower altitude but still above the ionospheric density peak. For instance, COSMIC and SWARM constellations are characterized by orbit altitude at about 700 and 500 km, respectively. In the case of tandems or satellites in close formation, VTECs can be considered as similar which can help to decorrelate and precisely recover receiver DCB and VTEC. The use of several satellites will contribute to reducing the uncertainty on DCBs by increasing the observability and improve the DCB stability with time, considering that satellite DCBs are constant values in time.

In addition to DCBs, the code-based VTEC extracted from our method can be used as an input of code leveling in TEC monitoring using phase measurements. Indeed, as the main issue in phase TEC monitoring is the calibration of code and phase delays, any valuable information concerning the TEC can help to improve the TEC recovery with phase measurements. At last, let us remember that this work relies on code observations only. This opens new perspectives considering the new generation signals which are more accurate than present ones, like the Galileo AltBOC modulation on the E5($a + b$) frequency which is characterized by a measurement noise several times lower than P-code and by increased resistance to multipath error. This research perspective would pave the way to TEC retrieval based on code measurements only.

Acknowledgements The authors would like to acknowledge the International GNSS Service (IGS) for providing orbits and RINEX data of its high-quality network of permanent stations. They would also thank all colleagues from Centre National d'Etudes Spatiales (CNES) in Toulouse for the interesting discussions and advice while writing and revising this work. In particular, they thank Gérard Zaouche for providing hardware temperature data of GPSP-B instrument onboard JASON-2.

References

AVISO website. http://www.aviso.altimetry.fr/fr/donnees/calval/orbit/precise-orbit-determination-verification.html

Banville S, Collins P, Zhang W, Langley RB (2013) Global and regional ionospheric corrections for faster PPP convergence. Navigation 61(2):115–124

Foelsche U, Kirchengast G (2002) A simple "geometric" mapping function for the hydrostatic delay at radio frequencies and

assessment of its performance. Geophys Res Lett. doi:10.1029/2001gl012744
Gulyaeva TL, Huang X, Reinisch B (2002) Ionosphere-plasmasphere model software for ISO. Acta Geod Geophys Hung 37(2–3):143–152
Hernández-Pajares M, Juan JM, Sanz J, Orús R (2007) Second-order ionospheric term in GPS: implementation and impact on geodetic estimates. J Geophys Res. doi:10.1029/2006JB004707
Hernández-Pajares M, Juan JM, Sanz J, Orus R, Garcia-Rigo A, Feltens J, Komjathy A, Shaer SC, Krankowski A (2009) The IGS VTEC maps: a reliable source of ionospheric information since 1998. J Geod 83(3):263–275
Hofmann-Wellenhof B, Lichtenegger H, Collins J (2001) GPS theory and practice, 5, revised edn. Springer, Wien
Klobuchar JA (1996) Ionospheric effects on GPS. In: Parkinson BW, Spilker JJ (eds) Global positioning system: theory and applications, chapter 12, vol 1. American Institute of Aeronautics and Astronautics, New York, pp 485–515
Lee HB, Jee G, Kim YH, Shim JS (2013) Characteristics of global plasmaspheric TEC in comparison with the ionosphere simultaneously observed by Jason-1 satellite. J Geophys Res 118:935–946. doi:10.1002/jgra.50130
Lin J, Yue X, Zhao S (2016) Estimation and analysis of GPS satellite DCB based on LEO observations. GPS Solut 20(2):251–258
Liu L, Wan W, Ning B (2006) A study of the ionogram derived effective scale height around the ionospheric hmF2. Ann Geophys 24:851–860
Loyer S, Perosanz F, Mercier F, Capdeville H, Marty JC (2012) Zero-difference GPS ambiguity resolution at CNES–CLS IGS analysis center. J Geod 86(11):991–1003. doi:10.1007/s00190-012-0559-2
Marinov P, Kutiev I, Belehaki A, Tsagouri I (2015) Modeling the plasmasphere to topside ionosphere scale height ratio. J Space Weather Space Clim. doi:10.1051/swsc/2015028
Montenbruck O, Hauschild A, Steigenberger P (2014) Differential code bias estimation using multi-GNSS observations and global ionosphere maps. Navigation 61(3):191–201. doi:10.1002/navi.64
Wang N, Yuan Y, Li Z, Montenbruck O, Tan B (2015) Determination of differential code biases with multi-GNSS observations. J Geod 90(3):209–228
Xu G (2003) GPS theory, algorithms and applications. Springer, Berlin, Heidelberg, New York
Yizengaw E, Moldwin MB, Galvan D, Iijima BA, Komjathy A, Mannucci AJ (2008) Global plasmaspheric TEC and its relative contribution to GPS TEC. J Atmos Sol Terr Phys 70:1541–1548
Yue X, Schreiner WS, Hunt DC, Rocken C, Kuo YH (2011) Quantitative evaluation of the low earth orbit satellite based slant total electron content determination. Space Weather. doi:10.1029/2011SW000687
Zakharenkova I, Cherniak I (2016) How can GOCE and TerraSAR-X contribute to the topside ionosphere and plasmasphere research? Space Weather 13:271–285. doi:10.1002/2015SW001162
Zhong J, Lei J, Dou X, Yue X (2016) Is the long-term variation of the estimated GPS differential code biases associated with ionospheric variability? GPS Solut 20(3):313–319

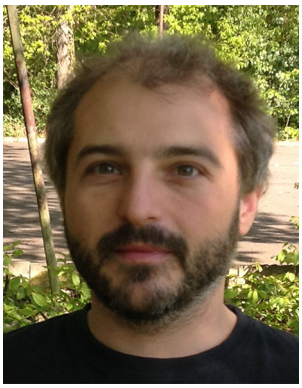

Gilles Wautelet obtained the Ph.D. degree which covered the study of the terrestrial ionosphere and its impact on precise positioning with GNSS from University of Liège, Belgium, in 2013. He worked as a research engineer within the space geodesy team at the Centre National d'Etudes Spatiales (CNES) in Toulouse, France, where this study was performed. He is currently a research fellow at the Space Sciences, Technologies and Astrophysics Research (STAR) Institute, at the University of Liège, Belgium. His research interests include the study of the ionosphere, precise positioning and the characterization of GNSS biases.

Sylvain Loyer works on all the aspects of GNSS processing (POD for GNSS and LEO, static or high frequencies PPP and Integer-PPP, GNSS software developments). Since 2008, he is in charge of CNES-CLS IGS Analysis Center final products. More recently, he is involved in the IGS Multi-GNSS-Experiment and produces GPS/GLONASS and Galileo precise orbits and clocks.

Flavien Mercier is senior expert in the CNES orbit determination team. Since 1999, his activities are mainly focused on precise orbit determination for altimetry satellites using GPS, Doris and SLR measurements (Topex, Jason). He is also a specialist in GPS processing, and he is participating to the CNES-CLS IGS Analysis Center and developed the method of zero difference ambiguity fixing (phase clocks), which is currently implemented in the CNES-CLS solution (grg) contributing to the IGS.

Félix Perosanz is a geodesist of CNES and is currently in charge of the CNES-CLS IGS Analysis Center at the GET/OMP laboratory in Toulouse, France. He received his Ph.D. in Geodesy at Toulouse University in 1995, and his current research focuses mainly on precise applications of GNSS such as satellite orbit determination, reference frame realization and Precise Point Positioning.